ASTFE

American Society
of Thermal and Fluids Engineers

SIMULATION OF NATURAL CONVECTION IN A SQUARE CAVITY WITH PARTIALLY HEATED AND COOLED VERTICAL WALLS

E. Evren Selamet[1], A. Selamet[2], and R. Dehner[3]

[1,3]Ohio State University, Center for Automotive Research, USA
[2]Ohio State University, Mechanical and Aerospace Engineering, USA

ABSTRACT

Natural convection driven by temperature differences between partially heated and cooled vertical walls in a square cavity is studied numerically. Steady or unsteady cellular flow structures and temperature patterns are illustrated along with the evolution of heat transfer rates in terms of Nusselt number. The cavity is filled with fluids of various Prandtl number, including .024 (liquid metal), .71 (air), 6 (water), and 450 (silicon oil). The effect of Prandtl and Rayleigh numbers on the flow regime and heat transfer is established along with two different thermal boundary conditions.

KEY WORDS: Natural convection, Prandtl number, Rayleigh number, instability

1. INTRODUCTION

The natural convection heat transfer has been the subject of the many studies since this phenomenon occurs in a wide variety of practical applications such as electronic equipment cooling, heat exchangers, solar collectors, and crystal growth. Following the classical work of Ostrach (1952), extensive experimental and numerical investigations have been conducted on both the heating and cooling aspects as applied to a combination of different geometries, boundary conditions, and fluids, leading to invaluable insight on buoyancy-driven flow regimes and heat transfer. Many focused on the well-known heat transfer physics in an enclosure with one wall maintained hot and the other (opposing wall) cold, while the remaining surfaces were kept adiabatic. Recently, natural convection in cavities with nonuniform wall temperature distribution received considerable attention due to its advantages in some engineering applications. Among these, relatively early work of Kubleck et al. (1980) and Poulikakos (1985) have studied natural convection in an air-filled rectangular enclosure with a single vertical wall accommodating both hot and cold regions (involving a step change in temperature in between) and the remaining three walls being adiabatic; Bilgen and Yedler (2007) considered a similar air-filled rectangular enclosure with one of side walls subjected to a sinusoidal temperature profile, while retaining the other three as adiabatic walls; also investigating an air-filled rectangular cavity, Deng and Chang (2008) imposed sinusoidal temperature distribution on side walls combined with adiabatic top and bottom walls. Sivasankaran and Pan (2014) investigated the effect of amplitude and phase deviation of sinusoidal temperature distribution of side walls in a cavity with adiabatic horizontal walls. More recently, Adnani et al. (2016) considered an air- and water-filled cavity with lower half of the side walls maintained hot and the upper half cold, while keeping top and bottom walls adiabatic.

The step change in wall temperature considered in some of the foregoing studies has motivated the present work. Recently, Evren-Selamet and her co-workers studied natural convection in square and elbow-shaped enclosures filled with air/liquid metal (2015), and finned cavities filled with air (2017) and liquid metal (2018). The objective of the current work is to expand on these steady/transient computational solutions in order to bring further insight into natural convection in a square cavity filled with variety of fluids where

*Corresponding Author: selamet.2@osu.edu

each of the two side walls is now subject to two different temperatures. One crude model for that type arrangement may be a closed area heated by some sort of heat sources on side walls and cooled off by windows. Following this brief Introduction, governing equations and boundary conditions are described next along with a brief referral to the numerical procedure. The results are discussed in Section 3, leading then to conclusions in the final section.

2. DEFINITION and FORMULATION

Present study considers a square cavity with two different boundary conditions as illustrated in Fig. 1: (a) lower halves of the side walls are maintained hot (at temperature T_H) and the upper halves cold (T_C); (b) left wall remains identical to Fig. 1a, while swapping hot and cold regions of the right wall, that is, now the upper half of right wall is hot and the lower half cold. Hereafter, these cases are referred to as BC1 and BC2, respectively. The top and bottom walls are both adiabatic.
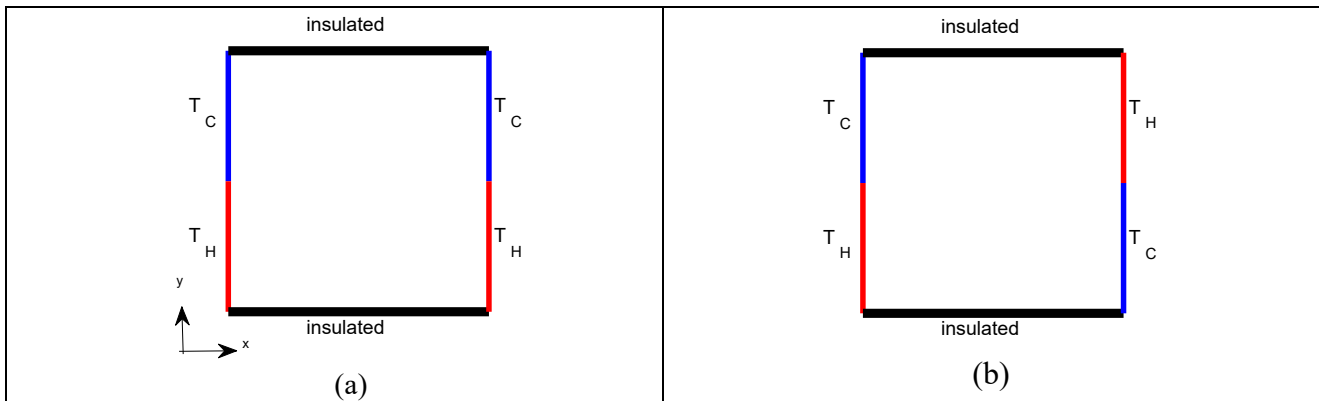

Fig. 1 Schematic of the cavity for two cases: (a) BC1 and (b) BC2.

In terms of the following dimensionless variables $x=x^*/L,\ y=y^*/L;\ u=u^*L/\alpha,\ v=v^*L/\alpha;\ t=t^*\alpha/L^2;$ $p=p^*L^2/(\rho\alpha^2);\ \theta=(T-T_c)/(T_h-T_c)$ where x^*, y^* are the coordinates; u^*, v^* the velocities; t^* the time; p^* the pressure; T the temperature; L the width of the enclosure, the governing equations for mass, x- and y-momentum, and energy may be written for buoyancy-driven incompressible fluids as

$$\frac{\partial u}{\partial x}+\frac{\partial v}{\partial y}=0,$$

$$\frac{\partial u}{\partial t}+\frac{\partial u^2}{\partial x}+\frac{\partial uv}{\partial y}=-\frac{\partial p}{\partial x}+\Pr\nabla^2 u,$$

$$\frac{\partial v}{\partial t}+\frac{\partial uv}{\partial x}+\frac{\partial v^2}{\partial y}=-\frac{\partial p}{\partial y}+\Pr\nabla^2 v+Ra\Pr\theta,$$

$$\frac{\partial \theta}{\partial t}+\frac{\partial u\theta}{\partial x}+\frac{\partial v\theta}{\partial y}=\nabla^2\theta,$$

where ∇^2 is the two-dimensional Laplacian; $\Pr=\nu/\alpha$, the Prandtl number; $Ra=g\beta\Delta TL^3/\nu\alpha$, the Rayleigh number which accounts for the coupling between energy and momentum balances, g being the gravitational acceleration, β the coefficient of thermal expansion of the fluid, ΔT the temperature difference between hot and cold boundaries; ν the kinematic viscosity; and α the thermal diffusivity. Boussinesq approximation, which treats density as a constant in all equations except for the gravitational force term in the momentum equation, is used. Even though the computations are performed by using primitive variables, flow field

results are presented in terms of the stream function Ψ ($u = \partial\Psi/\partial y$, $v = - \partial\Psi/\partial x$). No slip boundary conditions are imposed on all walls. Unsteady governing equations are employed here since the evolution of flow pattern and the associated temporal behavior can only be captured by using time-dependent computations. The governing equations with primitive variables are solved on a staggered grid (99x99) by a two-dimensional numerical scheme developed by the lead author applying the Godunov scheme to convective terms and centered finite difference to diffusive terms. Formulations of the problem and details of the method have been described in an earlier work [Evren-Selamet et al. (1992)]. Next, the computational results are presented.

3. RESULTS

The accuracy of the numerical approach employed in the present study has already been validated through earlier comparisons [see Evren-Selamet et al. (1992)] with the benchmark numerical solution of de Vahl Davis (1983), therefore such details will be avoided here. In addition, for the present case of BC1, one specific comparison is made with Adnani et al.'s work: an excellent agreement is observed in Fig. 2 which compares the present horizontal velocity profile in the middle of the cavity for Pr=.71 at Ra=10^5. Since Adnani et al.'s numerical solutions are based on steady-state governing equations, periodic or unsteady flow predictions found here are, however, not comparable with their study. For example, they predicted four counter-rotating cells of same size for Pr=7 at Ra=10^5, while the present study observes those cells periodically changing in size and shape due to the ability of time-dependent governing equations to capture the temporal physics.
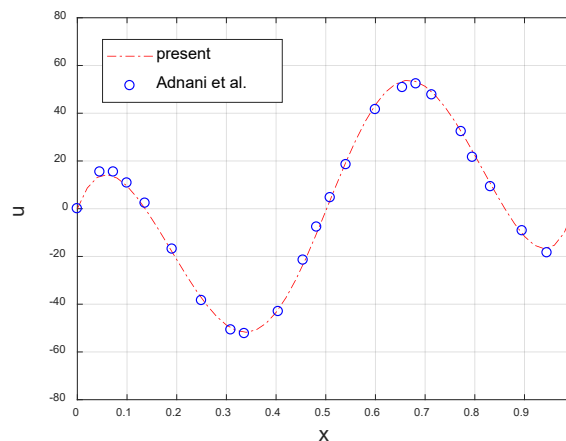

Fig. 2 Comparison of the horizontal velocity profile in the middle of the cavity for Pr=.71 and Ra=10^5, BC1.

Next, the results of the square cavity described earlier in Fig. 1 are presented in terms of streamlines and temperature profiles (isotherms), as well as the rate of heat transfer from the surfaces for Pr=.024 (liquid metal), .71 (air), 6 (water), and 450 (silicon oil) at Ra=10^4-10^6. Heat transfer rate is characterized by Nusselt (Nu) number which is the dimensionless temperature gradient integrated over the walls.

3.1 BC1

Solutions are obtained with various Pr and Ra to examine their effect. For Ra=10^4, (a) the streamlines and (b) isotherms are illustrated in Fig. 3 for Pr=.71 and 450. Flow and temperature fields for Pr=.024 and 6 are similar to those of Pr=.71 at Ra=10^4: four counter-rotating cells appear for Pr=.024, .71, and 6, while two counter-rotating cells for Pr=450. When Ra is increased to Ra=10^5 (Fig. 4), one main cell is now observed along with two corner cells in the flow field for Pr=.024; one elongated cell with two larger corner cells for Pr=.71; four-cell structure remains but with changing size and shapes for Pr=6 and 450 (not included in the figure) since flow now exhibits a time-dependent sinusoidal behavior. Single main vortex persists for Pr=.024 along with corner vortices of changing shape at all Ra considered here. Number of cells varies between 3 and 4 at Ra $\geq 3\times10^5$ and

Ra≥5x10^4 for Pr=.71 and 6, respectively, while it remains 4 for Pr=450. As a representative case of oscillating flows at Ra=10^6, Fig. 5 demonstrates the transition from 3 cells to 4 and then back to 3 in one cycle of periodic variation for Pr=6. Two convective cells first combine into one with time, which is then divided into two again with the pressure of growing two corner cells (top row). Bottom row shows corresponding isotherms which are confined to thin thermal boundary layer along the walls. Heat transfer is dictated primarily by those thermal boundary layers. Figure 6 depicts (a) the streamlines and (b) the isotherms for Pr=450 at Ra=10^6 at a specific time. The strengths of four cells all rotating opposite to each other change periodically. Isotherms again are concentrated along the walls. Next, the predictions associated with the second boundary condition (BC2) are discussed.
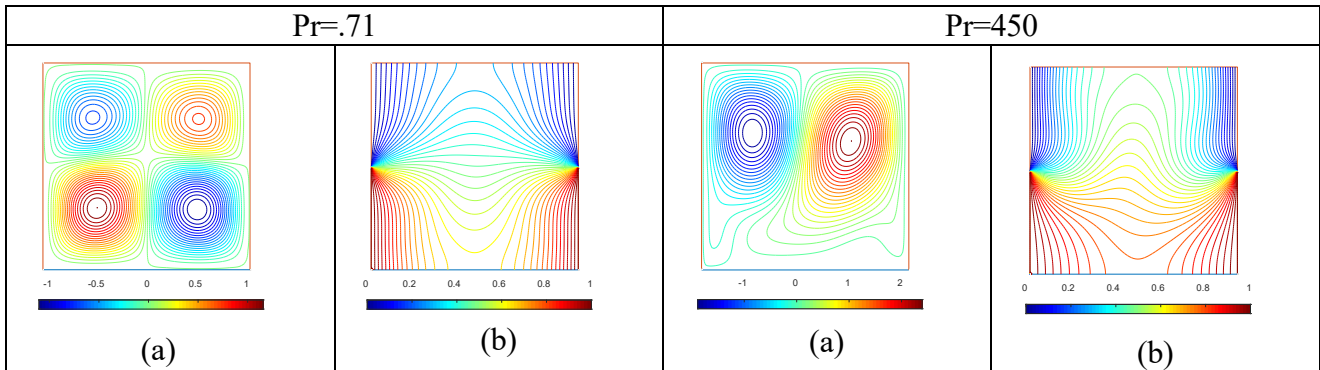

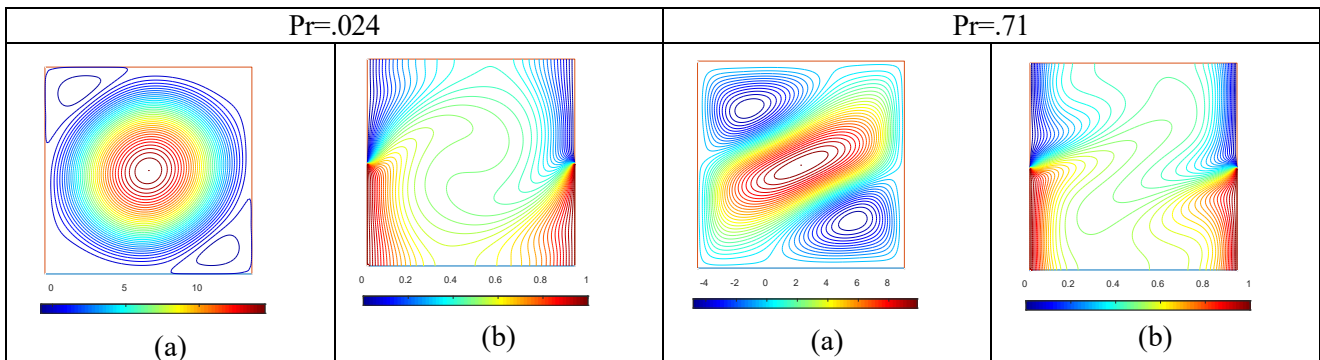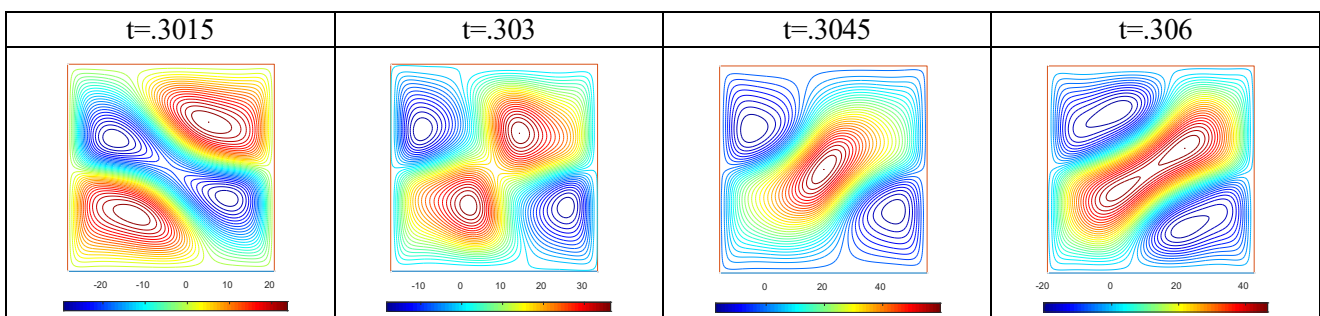**Fig. 3** (a) Streamlines and (b) isotherms for Pr=.71 and Pr=450 at Ra=10^4; BC1.

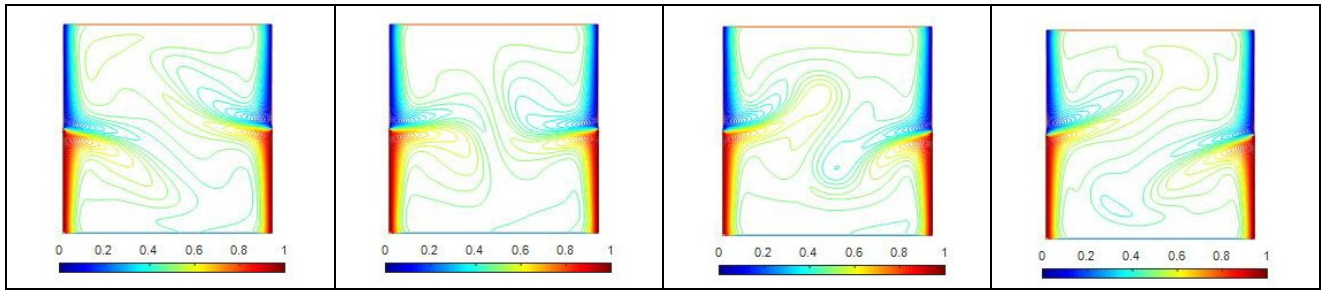**Fig. 4** (a) Streamlines and (b) isotherms for Pr=.024 and Pr=.71 at Ra=10^5; BC1.

Fig. 5 Transient pattern of streamlines (top row) and isotherms (bottom row) in one cycle of oscillation for Pr=6 and Ra=10^6.
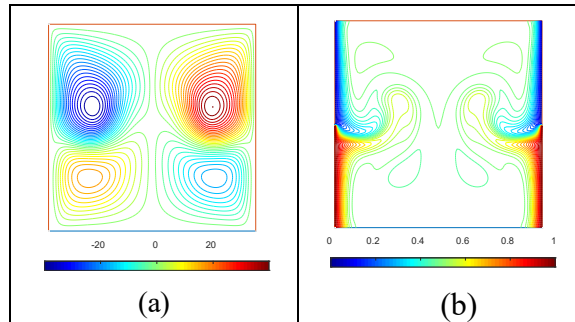

Fig. 6 (a) Streamlines and (b) isotherms at t=.25 for Pr=450 and Ra=10^6.

3.2 BC2

For this case, the bottom half of right wall is at a colder temperature than the top half (recall Fig. 1b). Unlike BC1, BC2 produces a pair of counter-rotating cells on top of each other for all Pr considered here. To save space, Fig. 7 represents (a) the streamlines and (b) the isotherms, only for Pr=.024 and .71 at Ra=10^5. The centers of circulating patterns are shifted to the right or left wall depending on Pr but both cells are symmetric about the mid-height. Isotherms are observed to be intense close to the walls. Higher Ra results in a similar structure but with two additional small cells inside the outer large cell. More stable solutions are obtained with this altered boundary condition for Pr=.71, 6, and 450. The evolution of Nu which represents the sum of the averaged heat transfer rate along the heated/cooled halves of both vertical side walls gives a clear picture of how modifying the boundary conditions from type 1 to 2 affects the heat transfer rate at various Pr and Ra.
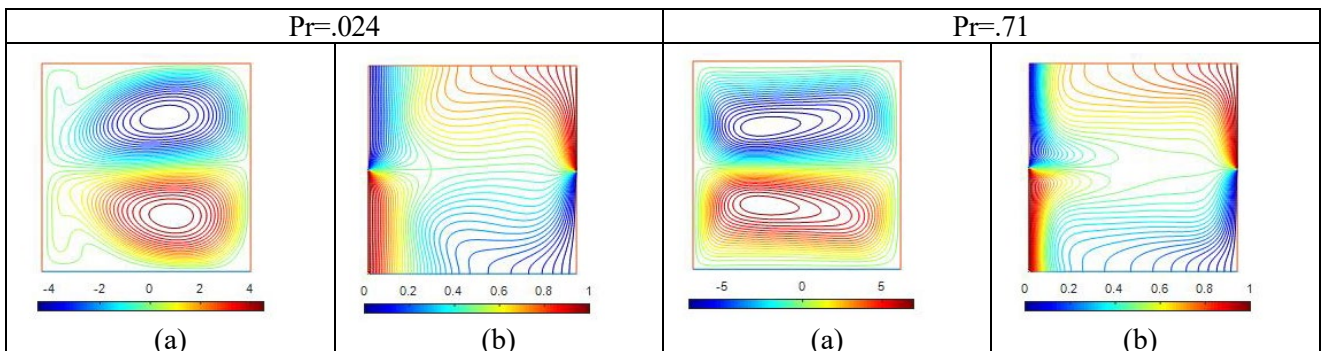

Fig. 7 Streamlines (a) and isotherms (b) for Pr=.024 and Pr=.71 at Ra=10^5; BC2.

Figure 8 compares the evolution of Nu_H with BC1 (maroon) and BC2 (green) for Pr=.024, .71, 6, and 450 at Ra=10^5, $3x10^5$, $5x10^5$, and 10^6. For Pr=.024, Nu_H for BC2 at Ra=10^5 shows early oscillatory behavior, and then reaches nearly a steady final value – same as BC1 which does not exhibit oscillations along the way. At higher Ra, both BC1 and BC2 show periodic oscillations: BC2 converges to an oscillatory behavior with its amplitude and mean Nu_H being higher than those of BC1. For Pr=.71, Nu_H at Ra=10^5 reaches a steady state smoothly for both types of boundary conditions; BC1 shows early symptoms of oscillations at Ra=$3x10^5$ with such oscillations growing at Ra=$5x10^5$ and becoming chaotic at Ra=10^6, whereas BC2 approaches a steady solution for all Ra considered. For Pr=.71, switching boundary condition from 1 to 2 not only increases the heat transfer rate but also stabilizes the flow field. Similarly, at Pr=6, Nu_H for BC2 remains higher than that of BC1. For BC1, Nu_H is periodic at Ra=10^5 and $3x10^5$, becoming nearly steady at higher Ra, whereas, for BC2, it is steady for all the discrete Ra considered here similar to Pr=.71. When Pr is increased further to 450, Nu_H shows regular sinusoidal variation at all Ra for BC1. BC2 again stabilizes the flow but the mean heat transfer rate is lowered slightly relative to BC1 at Ra=$5x10^5$ (and $7.5x10^5$ [not included in the figure]). The effects of two types of boundary conditions on the temporal variation of Nu_H are depicted in Fig. 9 at four different Pr and various Ra.
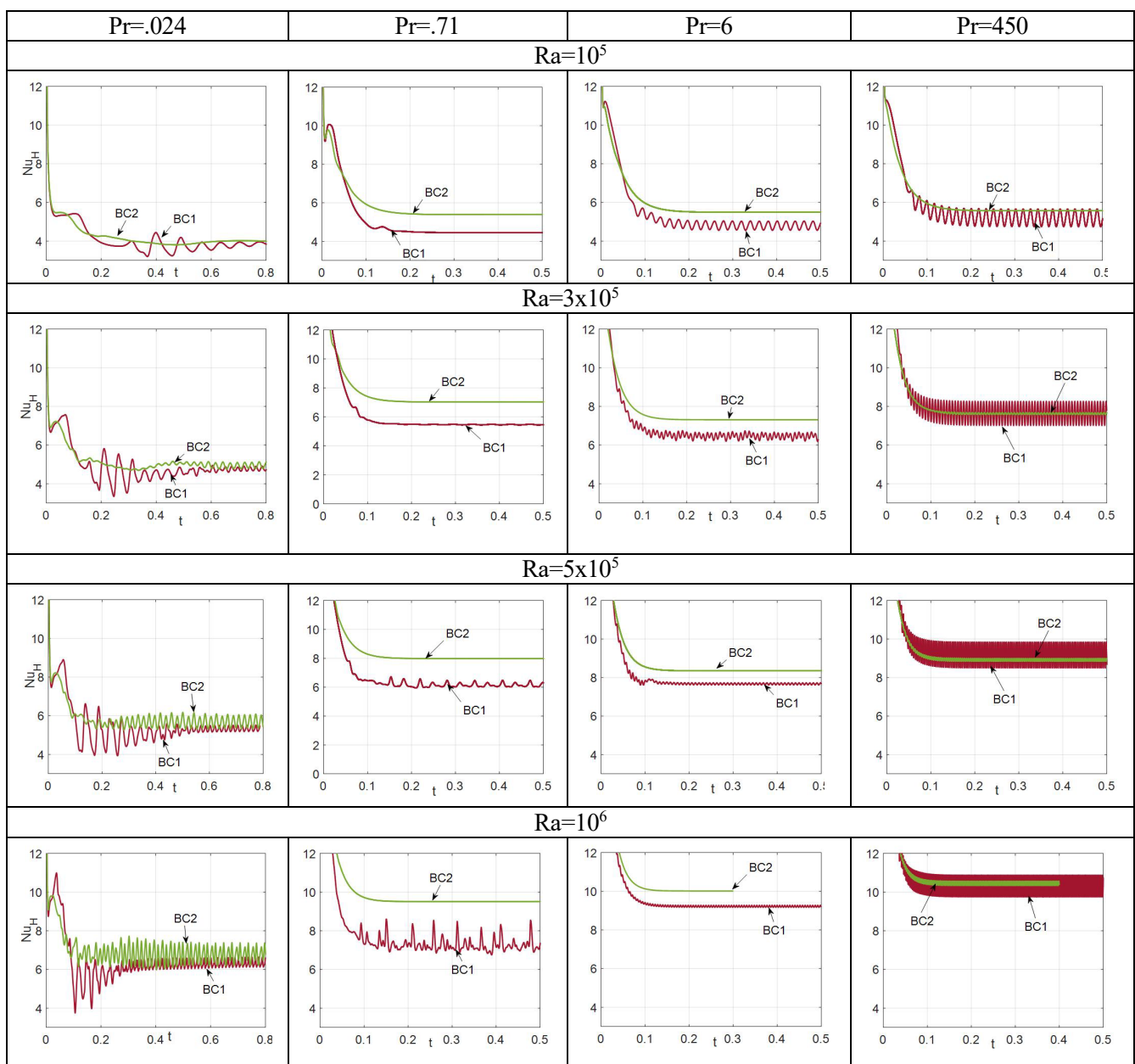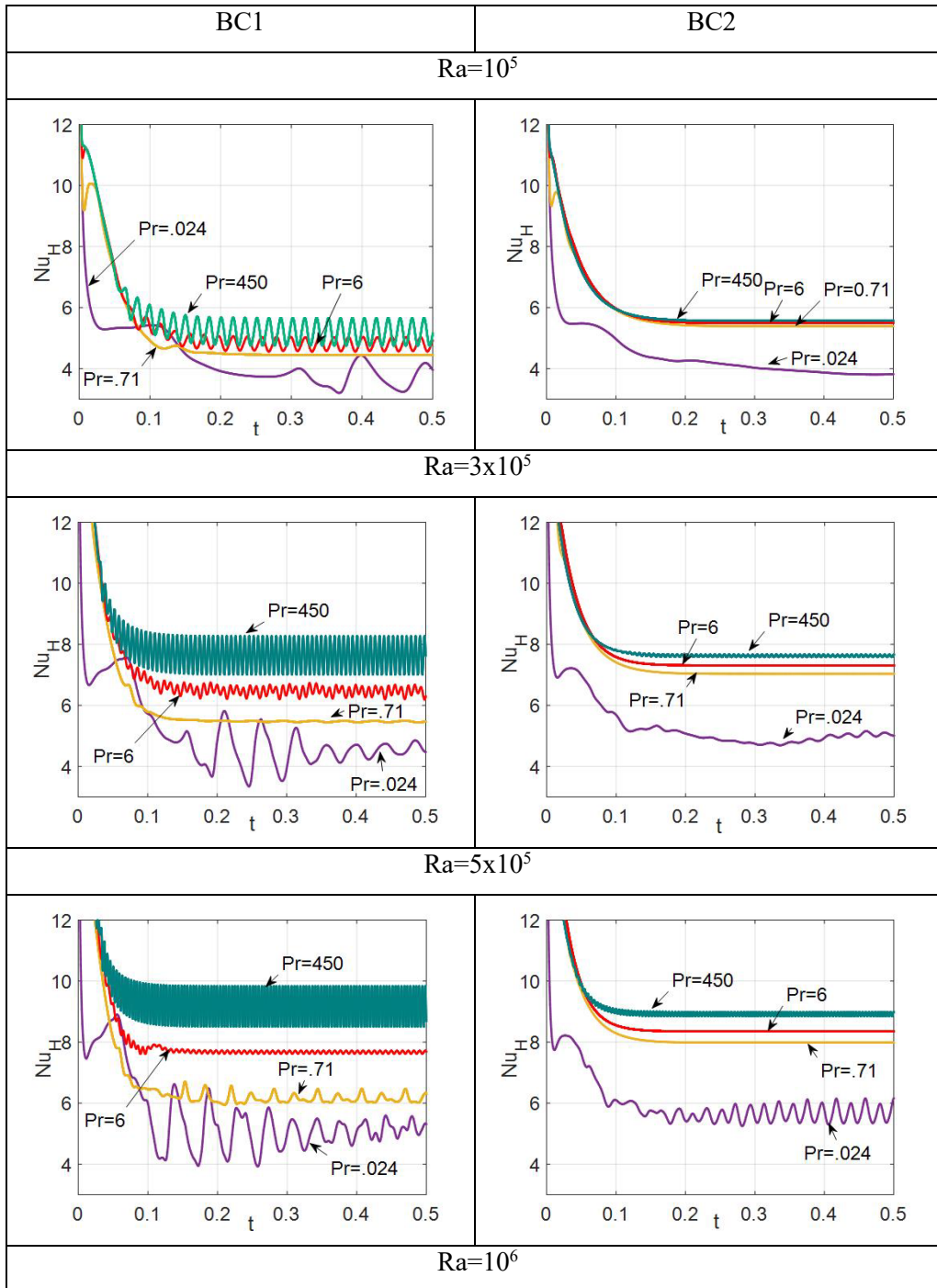
Fig. 8 Temporal variation of Nu$_H$ with two different boundary conditions for Pr=.024, .71, 6, and 450 at various Ra.

Examining the left column (BC1) and the right column (BC2) of Fig. 9 reveals that BC2 stabilizes the heat transfer and flow field for Pr=.71, 6, and 450 for all the cases considered here. This stabilizing effect did not occur for Pr=.024. Lowest Nu number is predicted with the smallest Pr number as it is expected due to much higher conductivity of the fluid.
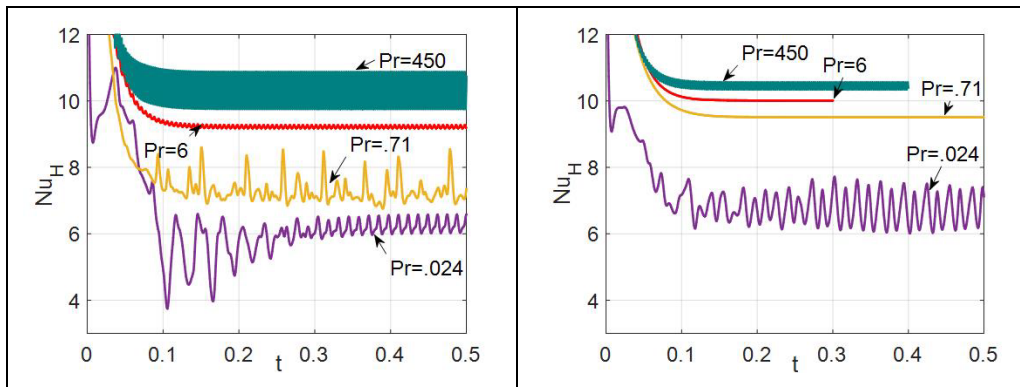
Fig. 9 Comparison of temporal variation of Nu_H with two different boundary conditions for Pr=.024, .71, 6 and 450 at various Ra.

Finally, mean value of Nu_H vs. Ra is shown in Fig. 10 for BC1 (solid line) and BC2 (dashed line) at four Pr used in this study. Most significant increase in Nu from BC1 to BC2 is obtained for Pr=.71 (blue) followed by Pr=6 (red) and Pr=.024 (magenta); Nu_H appears to decrease slightly (again from BC1 to BC2) for Pr=450 (green) around Ra=$5x10^5$ and $7.5x10^5$, in contrast to the behavior at smaller Pr. High viscosity of the silicon oil may be accountable for this behaviour. It is therefore concluded, from heat transfer enhancement viewpoint, that BC2 is most effective for Pr=.71 and 6, while also stabilizing the flow and temperature field. For these fluids BC2 alters the flow pattern from multi-cell to two-cell structure and energy transport by two cells appears better than that of multi cells leading enhancement of the average heat transfer rate inside the enclosure. This is also observed by Sivasankaran and Pan (2014).
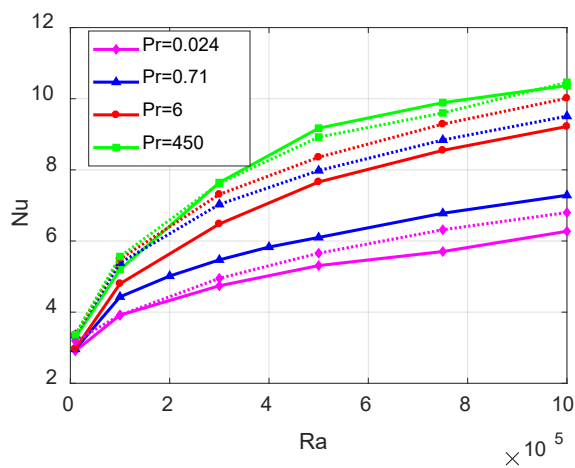

Fig. 10 Comparison of mean value of Nu_H for Pr=.024, .71, 6, and 450 vs. Ra for BC1 (solid line) and 2 (dashed line).

4. CONCLUSIONS

Natural convection driven by temperature differences between partially heated and cooled vertical walls in a square cavity is studied numerically. The effect of Pr and Ra on the flow regime and heat transfer is established along with two different thermal boundary conditions. BC2 is observed to stabilize the temperature and flow field for Pr=.71, 6, and 450 at all cases considered here. The trends with Pr=.024 are, however, not unidirectional: low Ra range manifests the similar stabilizing effect, yet, higher Ra range (Ra=$5x10^5$ and 10^6) maintains the oscillations, while also exhibiting a level of growth in amplitudes with time. BC2 is found to increase the heat transfer rate noticeably for Pr=.024, .71, and 6, with the most impact observed for Pr=.71.

REFERENCES

[1] S. Ostrach, "An Analysis of Laminar Free-Convection Flow and Heat Transfer About a Flat Plate," *NACA, TN 2635,* 1952.

[2] K. Kubleck, G. P. Merker and J. Straub, "Advanced Numerical Computation of Two-Dimensional Time-Dependent Free Convection in Cavities," *International Journal of Heat and Mass Transfer,* vol. 23, pp. 203-217, 1980.

[3] D. Poulikakos, "Natural Convection in a Confined Fluid-Filled Space Driven by a Single Vertical Wall with Warm and Cold Regions," *Journal of Heat Transfer,* vol. 107, pp. 867-876, 1985.

[4] E. Bilgen and R. B. Yeddler, "Natural Convection in Enclosure with Heating and Cooling by Sinusoidal Temperature Profiles one One Side," *Inernational Journal of Heat and Mass Transfer ,* vol. 50, pp. 139-150, 2007.

[5] Q. Deng and J. Chang, "Natural Convection in a Rectangular Enclosure with Sinusoidal Temperature Distributions on Both Side Walls," *Numerical Heat Transfer, Part A,* vol. 54, pp. 507-524, 2008.

[6] S. Sivasankaran and K. L. Pan, "Natural Convection of Nanofluids in a Cavity with Nonuniform Temperature Distributions on Side Walls," *Numerical Heat Transfer, Part A,* vol. 65, pp. 247-268, 2014.

[7] M. Adnani, B. Meziani, O. Ourrad and M. Zitoune, "Natural Convection in a Square Cavity: Numerical Study for Different Values of Prandtl Numbers," *Fluid Dynamics and Materials Processing,* vol. 12, no. 1, pp. 1-14, 2016.

[8] E. Evren-Selamet and A. Selamet, "Natural Convection for Air and Molten Gallium in Square- and Elbow-shaped Enclosures," *Applied Mechanics and Materials,* vol. 789, pp. 462-470, 2015.

[9] E. Evren-Selamet, A. Selamet and R. Dehner, "Effect of Fin Orientation and Length on the Rayleigh-Benard Convection," *Journal of Energy and Power Engineering,* vol. 11, pp. 317-335, 2017.

[10] E. Evren-Selamet, A. Selamet and R. Dehner, "Simulation of the Rayleigh-Benard Convection in a Finned Cavity Filled with Liquid Gallium," *3rd Thermal and Fluids Enginering Conference (TFEC),* pp. 551-560, 2018.

[11] E. Evren-Selamet V. S. Arpaci and C. Borgnakke, "Simulation of Laminar Buoyancy-driven Flows in an Enclosure," *Numerical Heat Transfer Part A,* vol. 22, pp. 401-420, 1992.

[12] G. V. Davis, "Natural Convection of Air in a Square Cavity: A Bench Mark Numerical Soluton," *Inernational Journal of Numerical Methods in Fluids,* vol. 3, no. 3, pp. 249-264, 1983.